A Physiologically Based Kinetic Model for Lead in Children and Adults

Ellen J. O'Flaherty

Department of Environmental Health, University of Cincinnati
College of Medicine, Cincinnati, Ohio

A physiologically based model of lead kinetics in children and adults has been developed and tested. The premises on which the physiologically based model is founded are reviewed in this paper. Because 95% or more of the body burden of lead in adults is found in the bone, bone metabolism is central to the model. Bone volumes are expressed as functions of body weight. Bone formation and resorption rates are estimated from human studies of stable labeled calcium kinetics. Cortical and trabecular bone are modeled separately, with their surface-to-volume ratios taken into account. Standardized growth curves are used to relate body weight to age. Other model features such as organ volumes and physiologic functions are related to body weight based on measurements made in human subjects over a range of ages. Calibrations of the model to two human data sets are shown, and two applications to specific research questions are illustrated. A brief comparison of the structure of this model with that of the Leggett model, and a comparison of the output of this model with that of the integrated exposure uptake biokinetic model of the U.S. Environmental Protection Agency, are also included. — *Environ Health Perspect* 106(Suppl 6):1495–1503 (1998). *http://ehpnet1.niehs.nih.gov/docs/1998/Suppl-6/1495-1503oflaherty/abstract.html*

Key words: lead, lead in children, IEUBK model, O'Flaherty model

A physiologically based model of lead kinetics in children and adults has been developed and tested. Several publications detailing its development and applications have appeared (*1–3*). The purposes of this paper are to review the premises on which the physiologically based model is built, to outline its relationship to bone metabolism, to depict some of its representations of physiologic functions, and to illustrate two of its applications. Brief comparisons of this model with that of Leggett (*4*) and with the integrated exposure uptake biokinetic (IEUBK) model of the U.S. Environmental Protection Agency (U.S. EPA) (*5*) are also included.

Bone Physiology and Metabolism

Total bone is conventionally considered to be about 20% trabecular bone and 80%

cortical bone (*6,7*). Although there actually exists a spectrum of bone compositions lying between prototypical cortical and prototypical trabecular bone, the traditional division into two bone types is a useful one for modeling purposes.

Bone near the center of long bones (the diaphyseal region of long bone) is typical of cortical bone. Figure 1 is a set of schematic drawings of growing and mature cortical long bone in dogs, based on microradiographs from Lee et al. (*8*). As the long bone grows (Figure 1A, B), its diameter is enlarged by the deposition of concentric lamellae at the outer (periosteal) surface and the accompanying enlargement of its marrow cavity by active bone resorption at the inner (endosteal) surface. These processes are integral components of the modeling that shapes growing bone. Mature diaphyseal bone, on the other hand (Figure 1C, D), no longer displays the ragged endosteal surface that indicates active bone resorption. Instead, mature cortical bone is constantly renewed through the process of remodeling, in which cavities are excavated in existing bone by the action of osteoclasts. Each of these cavities is gradually filled with new bone by the action of osteoblasts. The open channel remaining in the center, the haversian canal, carries a blood vessel. The unit containing the

haversian canal and the surrounding bone nourished by its blood vessel is an osteon.

Portions of two osteons are shown enlarged in Figure 2. Formation of new osteons appears to proceed without regard for the boundaries of existing osteons. Bone is laid down in the new osteon in lamellae, beginning at the periphery and moving in. Between the lamellae are cavities, or lacunae, which contain bone cells called osteocytes. The osteocytes are nourished via canalicules that radiate from each lacuna, connecting the spaces between lamellae with the haversian canal. These canalicules are the smallest of the channels that supply bone tissue with nutrients.

Bone in the interior of the vertebrae is typical of trabecular bone (Figure 3). Trabecular bone takes the form of narrow plates and struts having a much greater surface-to-volume ratio than cortical bone. Mature trabecular bone displays little or no osteonal remodeling activity. It is renewed by surface remodeling, which replaces and restructures it in response to a variety of factors including physical stresses. Loss of trabecular bone is largely responsible for the fragility of vertebral and hip bones in osteoporosis.

Table 1 gives an overview of some of the important features of bone physiology from the standpoint of devising a model of bone metabolism. Surface-to-volume ratios in trabecular bone are 5 to 6 times those in cortical bone, whereas cortical bone volume is 4 times that of trabecular bone. These physical features of bone appear to be reasonably species independent. If bone remodeling activity were assumed to be proportional to total surface area, then from 55 to 60% of total mature bone remodeling activity would be assigned to trabecular bone.

Total mature bone remodeling activity, however, is markedly species dependent. Small animals like mice and rats, with relatively short lifespans, display little cortical bone remodeling activity as adults. Presumably the need to replace aging cortical bone in these species is less acute. Recent studies in humans and in cynomolgus monkeys suggest that bone turnover is comparable in these two species. Although a range of bone turnover rates is found in both cortical and trabecular bone, reflecting the range of bone structures as well as other regional differences, the ranges observed in the monkeys (*9,10*) are consistent with experimental estimates of total turnover in mature human bone (Table 1).

Lead and Calcium Metabolism

Bone turnover is usually expressed as the mass of calcium exchanged per unit time. Early histomorphometric studies linked bone lead metabolism to that of calcium. In 1933, in a series of experiments in which the localization of lead in bone was compared to that of calcium, it was observed that

It was apparent that lead is always deposited where mobilizable calcium deposits are found. (11)

The link was made more explicit by other investigators.

After 11 days [of feeding lead to young guinea pigs], lead deposits [in the diaphysis of the femur] . . . consisted of a broad subperiosteal zone, a narrow subendosteal zone, and broad zones around the vascular channels. [In addition,] . . . a fine radiating structure was visible, especially around distant lacunae. (12)

In long bones of adult guinea pigs, . . . the predominant deposit is now in the subperiosteal lamellar region. Cortical areas bordering on marrow space contain little lead. Haversian and Volkmann's canals are lined with lead . .

. . Similarly, lead is present in bone cells and bone canaliculi. (12)

The studies showed that lead was being deposited on bone surfaces in general, and on surfaces engaged in modeling and remodeling in particular:

While in acute experimental lead poisoning lead is predominantly deposited in the subperiosteal zone and in the vicinity of the Haversian canals, the localization of normal lead in humans is strikingly different . . . . These patterns [of "normal" lead deposition] are so striking that the question of their origin asserts itself. It is likely that the answer is linked to bone remodeling. (13)
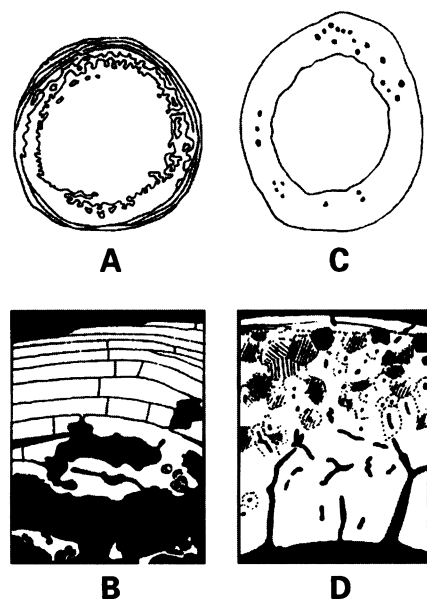

Figure 1. Transverse sections of femur midshaft from a puppy (A,B) and a mature dog (C,D). Fully calcified bone is white in these drawings; less fully calcified bone is denoted by degrees of shading. Note in Figure 1D that as the new osteons are filled in by freshly apposed bone mineral, the haversian canals that carry the blood vessels become narrower. Because of the general orientation of the haversian canals, most of the channels are cut transversely, but some are cut longitudinally. Drawings based on microradiographs from Lee et al. (8).
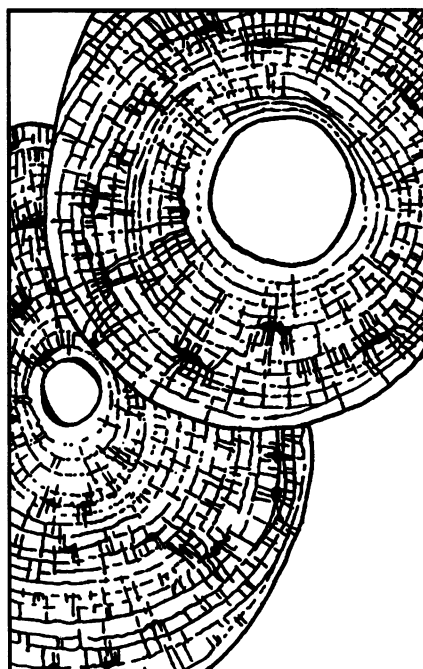

Figure 2. Portions of two osteons. The older osteon has been replaced in part by the younger one, which is not yet fully filled in. Drawing based on photomicrograph from Alberts et al. (51).
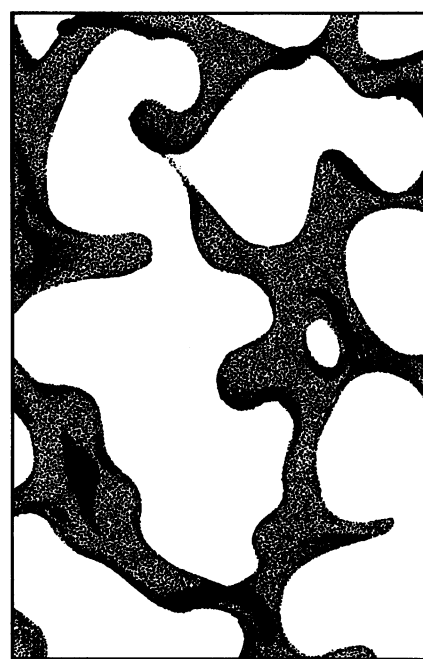

Figure 3. The structure of trabecular bone. A network of connecting narrow plates and struts creates a bone mesh with a high surface-to-volume ratio.

Table 1. Bone physiology and metabolism.

	Total bone	Cortical bone	Trabecular bone	References
Relatively species-independent characteristics				
Volume fraction, %	100	80	20	(6,7)
Surface-to-volume ratio, cm^2/cm^3	—	40–50[a]	100–250[b]	(29–40)
Blood flow	—	Proportional to bone formation rate	Proportional to bone formation rate	(41–43)
Species-dependent characteristics				
Turnover rate of mature bone, %/year				
Human	10	2–6	10–26	See below[c]
Cynomolgus monkey		1–12 (100%/year, iliac crest)	30–50 (40%/year, iliac crest)	(9,10)

[a]Includes periosteal, endosteal, and haversian canal surfaces. [b]Lower values generally associated with vertebral bone, higher values with iliac crest. [c]For total skeleton, see references (42–49). For cortical and trabecular bone: encapsulation of literature data is found in Legett et al. (50).

These early studies of lead distribution in bone, associating it with surface deposition and incorporation into forming bone, were more qualitative than quantitative. A third mechanism of uptake of lead into bone was defined more precisely in studies with uranium and radium isotopes and with isotopes of calcium itself. In one experiment, [233]U was administered to young adult beagles and its distribution in bone was evaluated between 1 and 726 days later. In cortical bone,

> Initially uranium is seen on endosteal and periosteal surfaces and lining the Haversian canals. As a function of time postinjection, the intensity of the surface label decreases and the cortical bone volume acquires a diffuse, uniform deposit. (14)

In trabecular bone,

> Low magnification images show the transition of an initially heterogeneous surface deposit at 1 day to a pattern in which the dense deposits are diminished as a function of time in number but not in intensity. Higher magnification emphasizes the heterogeneous character of the early deposits and a subsequent gradual redistribution from surfaces to bone volume. (14)

This redistribution of bone volume-seeking elements, a group that includes lead, throughout bone can be visualized as a heteroionic exchange of the elements with calcium (or an exchange of calcium with calcium) within the bone crystal matrix. Thus, surface exchange, deposition with forming bone, and slow migration throughout bone have all been implicated as mechanisms by which lead can become incorporated into bone.

Construction of Physiologically Based Lead Kinetics Model

The physiologically based lead kinetic model (hereafter called the O'Flaherty model) has been developed as a series of levels. The model of bone structure and age-dependent metabolism was designed first, then encapsulated by a model of age-related whole-body growth and metabolism. The behavior of lead within this shifting anatomic and physiologic framework was added next. Finally, an exposure module was constructed to try to capture the varieties of human lead exposure in as flexible a form as possible. The parameters associated with each of these levels were assigned values based on the best appropriate data sets from

the relevant literature. In a few instances, these data sets were from experimental animals rather than humans, but human data were relied on whenever possible. Parameters assigned values at each level were not allowed to change at the next or subsequent levels. With each model addition, only the new parameters were examined and assigned values.

The O'Flaherty model is based on body weight. All tissue volumes and blood flow rates, as well as bone turnover rates, are linked to body weight by means of expressions that reproduce physiologic measurements. For example, Figure 4 illustrates the volumes of liver and kidney as functions of body weight from birth to maturity (15). The departure of the kidney weights from linearity around 1 year of age is probably real but has not been explicitly modeled. Figure 5 illustrates the body weight dependence of the glomerular filtration rate (15,16). These data, as shown, were fit with two straight line segments. The change in slope occurs around 1 year of age, when standard body weight is 11.7 kg, which is also the age at which the deviation of body weight dependence of kidney weight from linearity is observed (Figure 4).

Some physiologic functions are different in males and females even after body weight has been taken into account. Figure 6 shows respiration rates for males and females as functions of body weight from birth to maturity (15). The data were fit with straight line segments, a single one for both males and females up to 1 year of age and separate line segments for males and females subsequent to that age.

Body weight is defined by five constants, two for the early childhood phase of growth and three for the subsequent adolescent growth spurt and stabilization at mature adult weight. Figure 7 shows body weight as a function of age for the white American female. The five constants allow other growth curves to be defined; for example, growth curves for specific ethnic or cultural groups or even for individuals. Once the growth curve has been specified, the other anatomic and physiologic features of the model have been defined as well.

Bone turnover is central to the model. It is responsible for incorporation of lead from blood plasma into forming bone and for return of lead from bone to plasma as bone is resorbed. Figure 8 shows bone formation rate as a function of age. The data are from a number of calcium isotope uptake studies, which provide estimates of the rates of new bone accretion. Bone
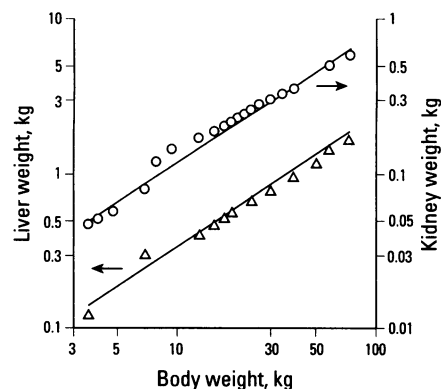

Figure 4. The volumes of liver (△; left axis) and kidneys (○; right axis) as functions of body weight in the human. Data are from Johnson et al. (15). The lines are the model simulations.
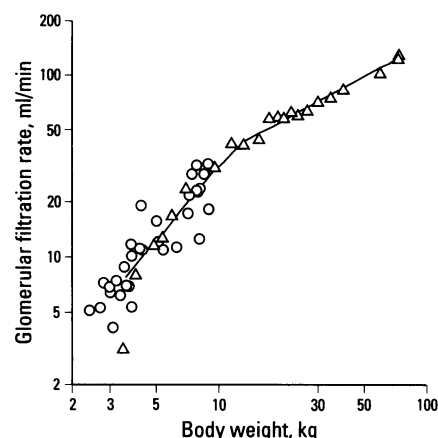

Figure 5. Glomerular filtration rate as a function of body weight. Data are from Johnson et al. (△)(15) and Rubin et al. (○)(16). The line is the model simulation.
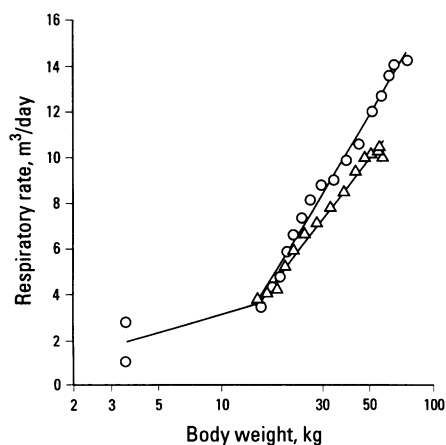

Figure 6. Respiration rate in males (○) and females (△) from birth to adulthood. Data are from Johnson et al. (15). The lines are the model simulations.

turnover is around 10% per year in the adult, independent of gender. In the model, 65% of total mature bone turnover is assigned to trabecular bone and 35% to cortical bone. Thus, mature trabecular bone turnover in the model is (0.65 × 0.10/0.2)/year, or 32.5% per year. Mature cortical bone turnover is (0.35 × 0.10/0.8), or between 4.3 and 4.4% per year. These percentages are consistent with the histomorphometric bone turnover data from adult cynomolgus monkeys (Table 1). They are higher than the values of 3% per year for cortical bone and 18% per year for trabecular bone based on strontium isotope kinetics and used by the International Commission on Radiological Protection (ICRP) (4,17,18), which would give a total bone turnover in adult humans of 6% per year.

Gender-specific differences in the age dependence of bone formation rate are to be expected around puberty, which girls generally experience earlier than boys. However, there are too few data points, particularly for girls, in this crucial age range (Figure 8) to define gender-specific curves on an empirical basis. The curves shown are based on an arbitrary difference modeled in the age at which the growth rate begins to slow, set at 10 years for girls and 11 years for boys. It is expected that these cutoff values, as well as the maximum rates of new bone accretion during adolescence, may be revised as new information about the timing and magnitude of the changes in these very rapid rates of bone growth becomes available.
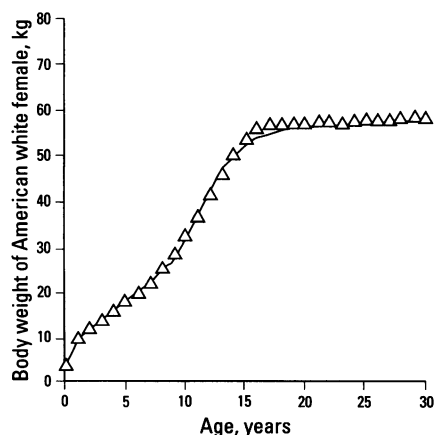
Because total bone volume is defined as a function of body weight, the expression for bone formation rate can be combined with the expression for net bone volume to generate an expression for bone resorption rate as a function of age or body weight. The two expressions, for bone formation rate and bone resorption rate, determine the rates of incorporation of lead into forming bone and loss of lead with resorbing bone. In addition, lead is allowed to diffuse into and throughout cortical bone in the model. Mathematically, this diffusion is expressed as a diffusion radially outward from the canalicules. Diffusion is not included in the trabecular bone compartment. Because of the thinness of the trabeculae in human bone and in the bone of smaller animals, haversian systems with their constituent canalicules are not present. The bone is supplied with nutrients directly from the marrow space.

Running the model is straightforward. The model includes exposure modules that allow the user to design exposure scenarios and to specify lead concentrations in air, food, water, dust, and soil. The exposure modules are similar to those in the U. S. EPA's IEUBK model for children. An important difference, however, is that background exposures in the O'Flaherty model are date dependent, reflecting the marked decreases in air and food lead that occurred during the 1970s and 1980s. Exposures can be changed during the course of a simulation run. Output concentrations in blood
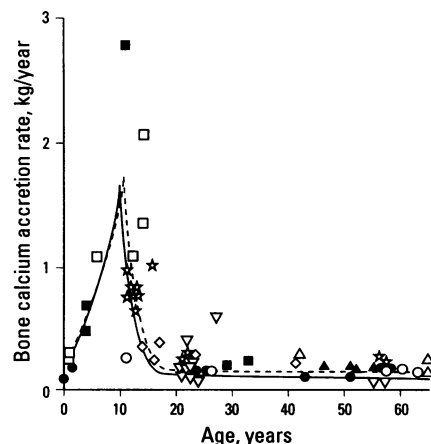
and tissues, including cortical and trabecular bone, can be accessed and plotted directly or imported into other graphical or spreadsheet software. The chief limitation of the model in its present form is that it is deterministic: model output does not include estimates of population distributions.

Extensions of the model to accommodate pregnancy and to incorporate the loss of bone that occurs with aging are planned.

Model Calibration

Two fits of the model to human data are illustrated in this section. It should be emphasized these are data set fits, in which parameters of the model were optimized during the fitting process. One example is for children, one for adults.

Figure 9 illustrates a model fit to one of the longitudinal data sets from the Cincinnati Prospective Lead Study (19). The group of children whose blood lead concentrations are shown here is the upper quartile of a large group that was followed from birth for over 6 years. These data were used to design the model expressions for soil and dust ingestion rates, illustrated in Figure 10. Dust ingestion was assumed to begin around age 3 months, to peak at age 2 years, and to fall off rather rapidly thereafter. Soil ingestion, an outdoor exposure, was assumed to begin at around age 6 months, to peak at age 3 years, and then to fall off fairly slowly with age as the child presumably continues to play outdoors and perhaps to participate in outdoor sports.

Figure 7. Body weight as a function of age in the human female. Data points are taken from a standardized growth chart for the American white female. The line is a model default growth curve.

Figure 8. Fractional bone formation rate as a function of age. The lines are the model simulations in males (dotted line) and females (solid line). Data are from Bronner and Harris (44) (☆); Bauer et al. (45) (○); Heaney and Whedon (46) (△); Bronner et al. (47) (◇); Neer et al. (48) (▽); and Abrams et al. (49) (□). Open symbols represent males; closed symbols represent females.

Figure 9. A model fit to the upper quartile of children in the Cincinnati Prospective Lead Study (19). The year of birth was set at 1983 for this simulation, drinking water lead concentration at 0.005 mg/l, soil lead concentration at 4100 ppm (g/g), and dust lead concentration at 1200 ppm. These blood lead concentration data were used to design the soil and dust ingestion curves shown in Figure 10. The line is the resulting model simulation.

Together, these two curves for soil and dust ingestion generate the blood lead concentration curve shown in Figure 9, which displays a rather sharp peak at age 2 years. The maximum blood lead concentration at age 2 years was a consistent feature of all quartiles in the Cincinnati Prospective Lead Study. It should be noted that lead uptake from soil and dust is determined by both age-dependent intake and age-dependent fractional absorption from the gastrointestinal tract. The curves illustrated in Figure 10 are coupled with a reasonable but somewhat uncertain expression, derived from an incomplete database, for age-dependent fractional lead absorption, which had been calibrated prior to addition of the exposure module to the model.

Figure 11 shows a simulation carried out in the course of general model calibration (2), for a 50-year-old male with workplace lead exposure superimposed on ambient exposure. The curve is made up of the end points of simulated 30-year exposures to a range of workplace air lead concentrations. The data points are from a study by Van de Vyver et al. (20) in which lead was assayed in ashed biopsy samples from the iliac crest of control and lead-exposed human subjects. As the simulated relationship is for a 30-year exposure, it would be expected to lie in the upper range of the experimental data, some of which would probably have represented shorter exposures. In addition, the simulation displays a degree of curvature that would not have been apparent from examination of the data alone but which nonetheless is entirely consistent with them.

Model Validation

Two examples of model validation will be given. These examples represent applications of the model to specific lead exposure issues without parameter adjustments. In both these examples, application of the model assisted in data resolution and interpretation.

The first example uses an earlier model version for the rat (21,22). One of the chief uncertainties associated with lead modeling is the wide range of lead bioavailability from exogenous oral sources. Some of this variability is associated with the chemical and physical nature of the source itself, and some with the conditions under which exposure occurs. For example, fractional absorption is substantially greater in the fasting state than in the fed state (23). A number of bioavailability studies have been reported. In a standard experimental design, animals are fed lead in the form of concern, usually for about 30 days, after which the concentrations of lead in blood, liver, kidney, and bone are compared to those in animals given daily intravenous doses of a soluble lead salt for 30 days. An estimate of fractional lead absorption is obtained for each tissue examined at each dose.

The physiologically based rat lead kinetic model has been applied to one such dataset (24). In this study (25), male and female rats were fed for 30 days a diet formulated with one of eight different lead concentrations. The source of the lead was two mine waste-containing soils, one with 5 times the lead concentration of the other. An intravenous lead acetate group was included (26). Bone, liver, and blood lead concentrations were measured at the end of

the 30-day exposure period. The model was fit to these data by optimizing the absorption rate constant for each group of rats at each dose level to achieve the best simultaneous fit to blood, liver, and bone lead concentrations. Thus, a single best estimate of fractional bioavailability was obtained from the three different tissue concentration measurements at each dose level (Table 2). (Note that tissue concentrations were judged to be indistinguishable from background concentrations at several of the low dose levels.)

Table 2 also gives the estimates of fractional bioavailability obtained by the conventional calculation, in which tissue concentrations were compared between oral and intravenous dose groups. As can be seen in the table, fractional bioavailability estimates vary widely, are tissue dependent, and display no apparent relationship to dose level. In addition, a disadvantage of this technique is that oral dose groups that generate tissue concentrations outside the range generated by intravenous dosing cannot be used in the calculations. Figure 12 demonstrates that fractional bioavailability estimated by application of the physiologically based model declines smoothly with dose from a high of 1.6% at the lowest dose to a low of 0.24% at the highest dose. Thus, the model integrates concentrations in different tissues into a single best estimate of fractional bioavailability at each dose, and by doing so reveals a clear-cut dose dependence of fractional bioavailability that was not previously apparent. The model can be applied at all dose rates at which tissue concentrations are distinguishable from background concentrations. In addition, because intravenous dose groups are not used, reliance on the model for estimation of fractional bioavailability reduces the number of animals required in a bioavailability study.

The second example application of the physiologically based lead model uses another version of the model. This version has been developed for the cynomolgus monkey, largely by scaling the human model to the body weight of the monkey. (The cynomolgus monkey skeleton is lighter in proportion to body weight than the human skeleton; actual data were used to model the monkey skeleton as a function of body weight in the scaled model.) This model version was applied to the results of a study in which adult female cynomolgus monkeys were administered stable lead isotopes sequentially, in order to label body stores of lead (almost exclusively
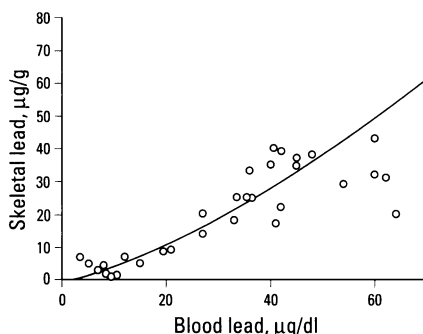
Figure 10. The modeled soil and dust ingestion rates. Together, these two curves generate the soil and dust contribution to the blood lead concentration curve shown in Figure 9.

Figure 11. Relationship between blood and bone lead for a 50-year-old male with workplace lead exposure superimposed on ambient exposure. Data are from Van de Vyver et al. (20). The line is the model simulation, made up of the end points of simulated 30-year exposures to a range of different workplace air lead concentrations.

Table 2. Absolute percentage bioavailability of lead from test soils added to feed (study 1).

Soil in diet, %	Lead in diet, ppm	Lead dose rate, mg/kg/day for 30 days		Percentage bioavailability: blood concentrations using standard method		Percentage bioavailability: bone concentrations using standard method		Percentage bioavailability: using PBK model	
		Males	Females	Males	Females	Males	Females	Males	Females
0.2	1.62 (soil I)	0.124	0.150	1.31 (9.04)[a]	2.07 (7.75)	0.36 (1.59)	0.39 (1.58)	—[b]	—[b]
0.5	4.05 (soil I)	0.314	0.501	2.29 (3.12)	5.72 (3.69)	0.48 (0.64)	0.58 (0.56)	—[b]	—[b]
0.2	7.82 (soil III)	0.680	0.916	1.27 (1.35)	2.23 (2.20)	0.087 (0.38)	0.36 (0.36)	1.60	—[b]
2	16.2 (soil I)	1.20	1.88	2.18 (0.82)	3.41 (1.23)	0.48 (0.25)	0.43 (0.18)	1.20	0.90
0.5	19.5 (soil III)	1.67	2.31	1.63 (0.57)	—[c]	0.35 (0.16)	—[c]	0.95	0.85
5	40.5 (soil I)	3.36	4.40	—[c]	—[c]	—[c]	—[c]	0.57	0.41
2	78.2 (soil III)	5.42	7.63	—[c]	—[c]	—[c]	—[c]	0.52	0.37
5	195 (soil III)	12.7	23.8	—[c]	—[c]	—[c]	—[c]	0.30	0.24

[a]Standard error in parentheses. [b]Not distinguishable from background exposure. [c]These calculations would have required extrapolation of intravenous dose concentration data.
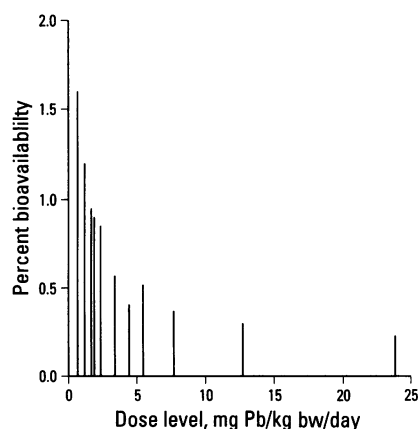
Figure 12. Percent absorption of lead from mine waste test soil treatment groups as a function of lead intake per unit body weight in male and female rats. Based on Polák et al. (24).
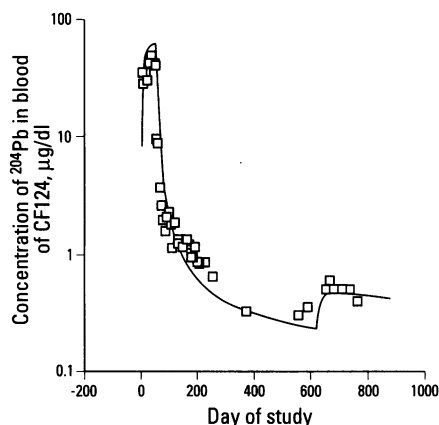
Figure 13. Concentration of a ^{204}Pb-enriched lead isotope mix in blood during the course of sequential administration of a series of isotope mixes to an adult female cynomolgus monkey. The line is the model simulation. See text for discussion.

bone lead) and thereby to distinguish between blood lead originating from past exposure and blood lead originating from current (dietary) lead (27). An observation made in this study was that on cessation of controlled lead exposure at the end of the isotope administration sequence, the blood concentrations of those lead isotopes administered earlier in the sequence, and therefore representative of endogenous lead, exhibited a transient but distinct rise, suggesting a shift to a new relationship between bone lead and blood lead (Figure 13). The data shown in Figure 13 are for a single isotope mixture enriched in ^{204}Pb. Administration of this isotope mix was begun on day 0 of the study and terminated on day 48. Lead exposure to other isotope mixes continued at an unchanged rate until exposure was terminated in this monkey on day 619 of the study. After day 619, total blood lead concentration, which is not shown, fell sharply from 40 to 45 µg/dl to 15 to 20 µg/dl. As illustrated in Figure 13,

the model predicts the observed rise in endogenous blood lead at this time, with subsequent continuation of the steady concentration decline at the rate observed before cessation of lead exposure. This shift in blood lead concentration does not represent a change in lead kinetics related to the abrupt drop in exposure, as might be inferred from the data alone. The model-predicted shift is caused by the nonlinearity of the relationship of red cell lead to plasma lead. Because lead is bound to a limited number of specific sites in the red cell, the capacity of the red cell to accommodate lead is limited. Although plasma lead is linearly related to exposure, red cell lead (and therefore blood lead) is not. At high blood lead concentrations, a larger fraction of total blood lead is present in the plasma than at low blood lead concentrations. Therefore, while plasma lead continues to decline smoothly after cessation of exposure in the situation modeled in Figure 13, readjustment of the equilibrium between

plasma and red cell lead as total blood lead falls results in a shift in the plasma lead–blood lead relationship to a higher blood lead concentration for a given plasma lead concentration.

Comparison with the Leggett/ICRP Model

Another physiologically based lead kinetic model has been developed and published (4). It was presented and discussed at the workshop at which this paper was also presented (28). The Leggett/ICRP model is an expansion of an ICRP age-specific model of lead metabolism (17,18). The ICRP model distinguishes between bone surface-seeking and bone volume-seeking elements, of which lead is bone volume-seeking. The Leggett/ICRP model does not include a diffusion mechanism for movement of lead throughout the bone volume. It accounts for the existence of an intermediate-term exchange process less explicitly, by designating an exchangeable bone volume and a nonexchangeable bone volume. With time, some of the lead in the exchangeable bone volume moves into the nonexchangeable bone volume, where it accumulates slowly and from which it can be returned to plasma only by bone resorption. The gradual transfer of lead from exchangeable to nonexchangeable pools accounts in the Leggett/ICRP model for a gradual decrease in rate of loss of lead from the skeleton as time since exposure increases. In sum, the Leggett/ICRP model assigns the time dependence of bone lead residence time to slow accumulation of a nonexchangeable lead pool, whereas the O'Flaherty model assigns the time-dependence of bone lead residence time to a gradual distancing of lead from bone surfaces by diffusion throughout the bone volume.

No exposure module is attached to the Leggett/ICRP model. Otherwise, the

Leggett/ICRP model is structurally analogous to the O'Flaherty model, although in a number of respects the Leggett/ICRP model is more complex. Exchanges between a diffusible plasma compartment and tissues except bone are considered to be first order, but a nonlinear relationship between plasma and red cell is included. Tissue uptake and loss are defined in terms of age-dependent transfer half-times, which are assigned values by interpolation between sequential ages for six different age groups. The gastrointestinal tract is modeled as four anatomically based segments, with absorption occurring only from the small intestine and fractional absorption being age-dependent stepwise rather than continuously. Liver and kidney both consist of two subcompartments. Lead in blood interchanges among a diffusible fraction, a plasma-bound fraction, and the red cells. Plasma-bound lead is not diffusible. With time, a gradual age-dependent shift of plasma-diffusible lead to plasma-bound lead takes place. Extravascular fluid is also a component of the model. Excretion takes place not only in urine and feces but also in sweat, hair, skin, and nails. Most of these differences between the two models are not critical to model function, although the assignment of different parameter values could cause model outputs to be different for the same set of exposure conditions. The Leggett/ICRP model has not been rigorously tested against datasets other than those on which it was based.

Comparison with the U.S. EPA IEUBK Model

The IEUBK model developed by the U.S. EPA is not physiologically based in the sense in which either the Leggett/ICRP model or the O'Flaherty model is. Although compartments are identified with tissues in the IEUBK model, it is primarily a descriptive model designed to reproduce blood lead concentrations in children up to 7 years of age, in typical urban exposure situations.

To compare the two models, the O'Flaherty model was run for the U.S. EPA lead exposure default conditions: outdoor air concentration 0.1 µg/m³ (the O'Flaherty model does not distinguish between outdoor and indoor air as the IEUBK model does); drinking water concentration, 4 µg/liter; soil and dust concentrations, each 200 µg/g; dietary uptake, age-dependent default daily rates; and no contribution from paint. Because

of the different ways in which dietary exposure data are entered in the two models (the IEUBK model uses age-dependent uptake rates in micrograms per day, whereas the O'Flaherty model uses date [year]-dependent intake rates and applies an age-dependent fractional absorption to them), the forms of the two curves for uptake of lead from food and water cannot be made congruent (Figure 14). Similarly, because the same age-dependent fractional absorption from the gastrointestinal tract is applied in the O'Flaherty model to lead originating from soil and dust, the curves for uptake of lead from soil and dust do

not have the same shape (Figure 15). Uptake of lead from air behaves in the same age-dependent fashion in the two models. Although it is greater in the O'Flaherty model than in the IEUBK model (Figure 16), it is a very minor contributor to blood lead overall under these default conditions. Despite these qualitative and quantitative differences in lead uptake, the two models give predicted blood lead concentrations that are not greatly dissimilar (Figure 17). This is not unexpected, as both models were calibrated against the same types of data for blood lead concentrations in urban children. It is
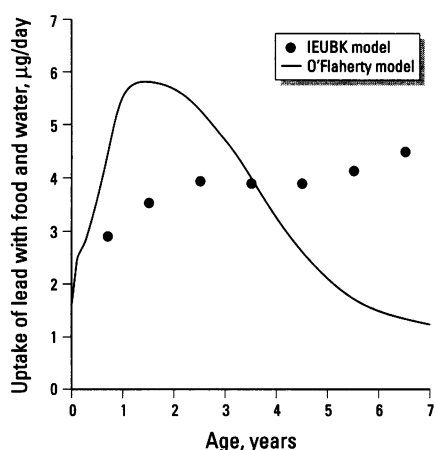

Figure 14. The rate of uptake of lead from food and drinking water as a function of age in children. IEUBK default values (points) and O'Flaherty model simulation (curve), with intake of lead in food in the O'Flaherty model designed to approximate as far as possible the range of IEUBK defaults.
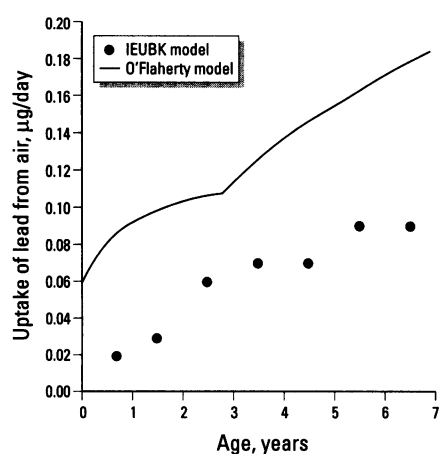

Figure 16. The rate of uptake of lead from air as a function of age in children. IEUBK default values (points) and O'Flaherty model simulation based on the IEUBK default concentration of 0.1 µg/m³ (curve).
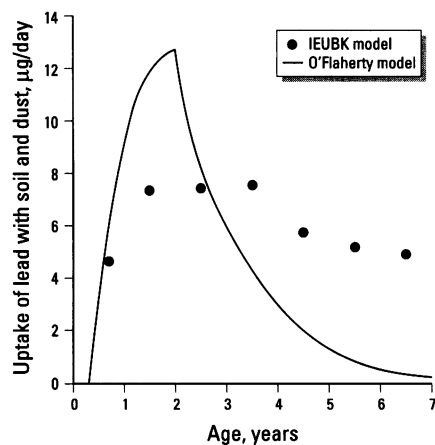

Figure 15. The rate of uptake of lead from soil and dust as a function of age in children. IEUBK default values (points) and O'Flaherty model simulation based on the IEUBK default concentration of 200 µg lead/g of both dust and soil (curve).
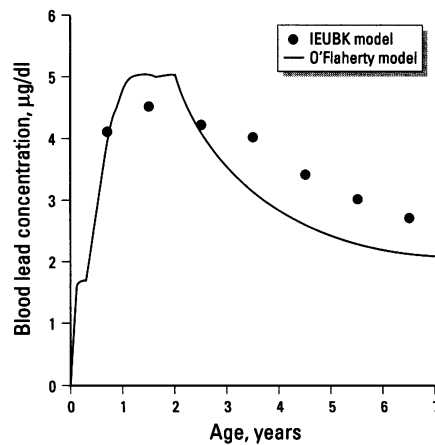

Figure 17. Blood lead concentration as a function of age in children. IEUBK model simulation (points) and O'Flaherty model simulation (curve). Simulations are based on the default uptake values illustrated in Figures 14–16.

an example of how highly parameterized models can yield similar results in spite of the assignment of different values to many of the parameters.

Comment

Ideally, the calibration and validation of any model should be entirely independent of each other. The calibration step(s) result in the assignment of values to the parameters of the model, with greater or lesser degrees of assurance depending on the quality of the databases relied on.

Validation is the comparison of model predictions for particular situations with observations made under the same conditions holding all parameter values constant. Models designed to predict future events may never be fully validated. However, models such as these, which are designed to predict the behavior of a biological system or organism under a specified set of conditions, are capable of validation in that they can be shown to perform well (or not well) under a variety of different sets of conditions. If they do

not perform adequately, then recalibration or, depending on the nature of the failure, model restructuring is in order. In a sense, then, calibration and validation are not entirely mutually independent exercises for models of this kind. Each process helps to inform the other. A validation failure may force model recalibration or redesign, whereas the process of calibration may pinpoint areas of uncertainty and suggest validation exercises specifically designed to examine model performance in these areas.

REFERENCES AND NOTES

1. O'Flaherty E J. Physiologically-based models for bone-seeking elements. III: Human skeletal and bone growth. Toxicol Appl Pharmacol 111:332–341 (1991).
2. O'Flaherty EJ. Physiologically-based models for bone-seeking elements. IV: Kinetics of lead disposition in humans. Toxicol Appl Pharmacol 118:16–29 (1993).
3. O'Flaherty EJ. Physiologically-based models for bone-seeking elements. V: Lead absorption and disposition in childhood. Toxicol Appl Pharmacol 131:297–308 (1995) .
4. Leggett R. An age-specific kinetic model of lead metabolism in humans. Environ Health Perspect 101:598–616 (1993).
5. U.S. EPA. IEUBK. Guidance Manual for the Integrated Exposure Uptake Biokinetic Model for Lead in Children. EPA/540/R-93/081; Washington: U.S. Environmental Protection Agency, 1994.
6. Gong JK, Arnold JS, Cohn SH. Composition of trabecular and cortical bone. Anat Rec 149:325–332 (1964).
7. Johnson, LC. In: Bone Biodyamics (Frost HM, ed). New York:Little, Brown, 1964;543–654.
8. Lee WF, Marshall JH, Sissons HA. Calcium accretion and bone formation in dogs. J Bone Joint Surg 47B:157–180 (1965).
9. Jerome CP, Carlson CS, Register TC, Bain FT, Jayo MJ, Weaver DS, Adams MR. Bone functional changes in intact, ovariectomized, and ovariectomized, hormone-supplemented adult cynomolgus monkeys (Macaca fascicularis) evaluated by serum markers and dynamic histomorphometry. J Bone Miner Res 9:527–540 (1994).
10. Jerome CP. Personal communication.
11. Behrens B, Baumann A. Zur Pharmakologie des Bleis. X: Die Beziehung der Bleiablagerung zum Calciumstoffwechsel. Z Ges Exp Med 92:251–264 (1933).
12. Sieber S. Histochemischer Bleinachweis im Knochen. Z Exp Med 181:273–280 (1936) .
13. Timm F. Der Histochemische Nachweis des "Normalen" Bleis in Menschlichen Hartgeweben. Virchows Arch 297:502–507 (1936).
14. Stevens W, Bruenger FW, Atherton DR, Smith JM, Taylor GN. The distribution and retention of hexavalent ^{233}U in the beagle. Radiat Res 83:109–126 (1980). .
15. Johnson TR, Moore WM, Jeffries JE, eds. Children Are Different: Developmental Physiology. Columbus, OH:Ross Laboratories, 1978.
16. Rubin MI, Bruck E, Rapoport M. Maturation of renal function in childhood: clearance studies. J Clin Invest 28:1144–1162 (1949).
17. International Commission on Radiological Protection. Age-Dependent Doses to Members of the Public from Intake of Radionuclides. ICRP Publ 56, Part 1. Oxford:Pergamon Press, 1989.

18. International Commission on Radiological Protection. Age-Dependent Doses to Members of the Public from Intake of Radionuclides. ICRP Publ 56, Part 2. Oxford:Pergamon Press, 1993.
19. Dietrich KN, Berger OG, Succop PA.. Lead exposure and the motor developmental status of urban six-year-old children in the Cincinnati Prospective Study. Pediatrics 91:301–307 (1993).
20. Van de Vyver FL, D'Haese PC, Visser WJ, Elseviers MM, Knippenberg LJ, Lamberts LV, Wedeen RP, DeBroe ME. Bone lead in dialysis patients. Kidney Int 33:601–607 (1988).
21. O'Flaherty EJ. Physiologically-based models for bone-seeking elements. I: Rat skeletal and bone growth. Toxicol Appl Pharmacol 111:299–312 (1991).
22. O'Flaherty EJ. Physiologically-based models for bone-seeking elements. II: Kinetics of lead disposition in rats. Toxicol Appl Pharmacol 111:313–331 (1991).
23. Rabinowitz MB, Kopple JD, Wetherill GW. Effect of food intake and fasting on gastrointestinal lead absorption in humans. Am J Clin Nutr 33:1784–1788 (1980).
24. Polák J, O'Flaherty EJ, Freeman GB, Johnson JD, Liao, SC, Bergstrom PD. Evaluating lead bioavailability data by means of a physiologically based lead kinetic model. Fundam Appl Toxicol 29:63–70 (1996).
25. Freeman GB, Johnson JD, Killinger JM, Liao SC, Feder PI, Davis AO, Ruby MV, Chaney RL, Lovre SC, Bergstrom, PD. Relative bioavailability of lead from mining waste soil in rats. Fundam Appl Toxicol 19:383–398 (1992).
26. Freeman GB, Johnson JD, Liao SC, Feder PI, Davis AO, Ruby MV, Schoof RA, Chaney RL, Bergstrom PD. Absolute bioavailability of lead acetate and mining waste lead in rats. Toxicology 91:151–163 (1994).
27. Inskip MJ, Franklin CA, Baccanale CL, Manton WI, O'Flaherty EJ, Edwards CMH, Blenkinsop JB, Edwards EB. Measurement of the flux of lead from bone to blood in a non-human primate (Macaca fascicularis) by sequential administration of stable lead isotopes. Fundam Appl Toxicol 33:235–245(1996).
28. Pounds JG, Leggett RW (1998). The ICRP age-specific biokinetic model for lead: validation, empirical comparisons, and explorations. Environ Health Perspect 106(Suppl 6): 1505–1511 (1998).
29. Bromley RG, Dock NL, Arno JS, Jee WSS. Quantitative histological study of human lumbar vertebrae. J Gerontol 21: 537–543 (1966).
30. Dunnill MS, Anderson JA, Whitehead R. Quantitative histological studies on age changes in bone. J Pathol Bacteriol 94:275–291 (1967).
31. Lloyd E, Rowland RE, Hodges D, Marshall JH. Surface to volume ratios of bone determined by computer analysis of microradiographs. Nature 218:365–366 (1968).

32. Amstutz HC, Sissons HA. The structure of the vertebral spongiosa. J Bone Joint Surg Br 51B:540–550 (1969).

33. Dyson ED, Jackson CK, Whitehouse WJ. Scanning electron microscope studies of human trabecular bone. Nature 225:957–959 (1970).

34. Merz WA, Schenk RK. Quantitative structural analysis of human cancellous bone. Acta Anat 75:54–66 (1970).

35. Lloyd E, Hodges D. Quantitative characterization of bone: a computer analysis of microradiographs. Clin Orthop 78:230–250 (1971).

36. Beddoe AH, Darley PJ, Spiers FW. Measurements of trabecular bone structure in man. Phys Med Biol 21:589–607 (1976).

37. Beddoe AH. Measurements of the microscopic structure of cortical bone. Phys Med Biol 22:298–308 (1977).

38. Vedi S, Compston JE, Webb A, Tighe JR. Histomorphometric analysis of dynamic parameters of trabecular bone formation in the iliac crest of normal British subjects. Metab Bone Dis Relat Res 5:69–74 (1983).

39. Sontag W. Quantitative measurements of periosteal and cortical-endosteal bone formation and resorption in the midshaft of female rat femur. Bone 7:55–62 (1986).

40. Sontag W. Quantitative measurements of periosteal and cortical-endosteal bone formation and resorption in the midshaft of male rat femur. Bone 7:63–70 (1986).

41. Sim FH, Kelly PJ. Relationship of bone remodeling, oxygen consumption, and blood flow in bone. J Bone Joint Surg 52A:1377–1389 (1970).

42. Whiteside LA, Simmon DJ, Lesker PA. Comparison of regional bone blood flow in areas with differing osteoblastic activity in the rabbit tibia. Clin Orthop Relat Res 124:267–270 (1977).

43. Niv AF, Hungerford DS. Bone blood flow in anesthetized and conscious dogs. Trans Orthop Res Soc 4:17 (1979).

44. Bronner F, Harris RS. Absorption and metabolism of calcium in human beings, studied with calcium45. Ann NY Acad Sci 64:314–325 (1956).

45. Bauer GCH, Carlsson A, Lindquist B. Bone salt metabolism in humans studied by means of radiocalcium. Acta Med Scand 158:143–151 (1957).

46. Heaney RP, Whedon GD. Radiocalcium studies of bone formation rate in human metabolic bone disease. J Clin Endocrinol Metab 18:1246–1267 (1958).

47. Bronner F, Richelle LJ, Saville PD, Nicholas JA, Cobb JR. Quantitation of calcium metabolism in postmenopausal osteoporosis and in scoliosis. J Clin Invest 42:898–908 (1963).

48. Neer R, Berman M, Fisher L, Rosenberg LE. Multicompartmental analysis of calcium kinetics in normal adult males. J Clin Invest 46:1364–1379 (1967).

49. Abrams SA, Esteban N., Vieira NE, Sidbury JB, Specker BL, Yergey AL. Developmental changes in children assessed using stable isotopes. J Bone Miner Res 7:287–293 (1992).

50. Leggett RW, Eckerman KF, Williams LR. Strontium-90 in bone: a case study in age-dependent dosimetric modeling. Health Phys 43:307–322 (1982).

51. Alberts B, Bray D, Lewis J, Raff M, Roberts K, Watson JD. Molecular Biology of the Cell. New York:Garland, 1983.